Proceedings of MSEC2012
2012 ASME International Conference on Manufacturing Science and Engineering
June 4-8, 2012, West Lafayette, IN

MSEC2012-7275

METHODOLOGY TO DETERMINE FRICTION IN ORTHOGONAL CUTTING WITH APPLICATION TO MACHINING TITANIUM AND NICKEL BASED ALLOYS

Durul Ulutan and Tuğrul Özel*
Manufacturing Automation Research Laboratory
Dept. of Industrial and Systems Engineering Rutgers University
Piscataway, NJ 08854 USA
ulutan@eden.rutgers.edu ozel@rci.rutgers.edu
*Corresponding author

ABSTRACT

Friction plays a very important role in machining titanium and nickel alloys. It is the source for the high amount of heat generation, and as a result, the excessive tool wear during machining these materials. The worn tool is known to create lower surface qualities with tensile surface residual stresses and machine-induced hardening at the surface, as well as high surface roughness. It is essential to create a method to determine how and to what extent the friction is built up on the tool. This study facilitates a determination methodology to estimate the friction coefficients between the tool and the chip on the rake face, as well as the tool and the workpiece on the flank face of the tool. The results are validated with experimental results from the titanium alloy Ti-6Al-4V and the nickel alloy IN-100.

1. INTRODUCTION

Machining difficult-to-process materials such as Titanium and Nickel-based alloys has been a major hurdle for manufacturing industry in terms of productivity for a significant amount of time, and there are a number of issues that are yet to be understood. The effect of friction is an important issue and as it is the case with many other materials, there is a lack of complete understanding in how friction plays role in machining Titanium and Nickel-based alloys. Let alone 3D machining processes, the work on friction in 2D orthogonal machining processes still lacks entirety. It is known that with increasing friction, heat buildup and tool wear increases especially in case of Titanium and Nickel based alloys due to their low thermal conductivity and chemical affinity with tool materials at elevated temperatures. Consequently there are surface integrity problems at the end product that will reduce product effectiveness, quality and reliability.

2. NOMENCLATURE

$a\text{-}h_{1\text{-}2}$	coefficients of the non-linear relationships
b	depth of cut
l_c	chip-tool contact length along the tool rake face
l_p	plastic contact length along the tool rake face
l_2	contact length along the flank face
F_c	total cutting force
F_f	total feed force
F_{c_0}	cutting force for the 3rd zone – ploughing component
F_{f_0}	feed force for the 3rd zone - ploughing component
F_{n_i}	normal force component at Region i
F_{t_i}	tangential force component at Region i
$F_{n_{i_c}}$	cutting force due to normal stresses at Region i
$F_{n_{i_c}}$	cutting force due to tangential stresses at Region i
$F_{n_{i_f}}$	feed force due to normal stresses at Region i
$F_{n_{i_f}}$	feed force due to tangential stresses at Region i
m	exponential coefficient for Region III
n	exponential coefficient for Region I
r_β	cutting edge radius
t_u	uncut chip thickness
VB	tool flank wear length
V_c	cutting speed
x_1	distance along the rake face from edge face
x_2	distance along the flank face from edge face
α	angle measured from horizontal direction for Region II
α_0	starting angle for Region II
α_f	final angle for Region II

γ_1	rake angle
γ_2	clearance angle
γ_s	stagnation point angle
θ	tool flank wear angle
μ	mean friction coefficient
μ_{ap}	apparent friction coefficient
μ_{sl}	sliding friction coefficient
μ_1	friction coefficient along the rake face
μ_2	friction coefficient along the flank face
σ_{n_1}	normal stress at the rake face
$\sigma_{n_{1_{max}}}$	maximum normal stress at the rake face
σ_{n_3}	normal stress at the flank face
$\sigma_{n_{3_{max}}}$	maximum normal stress at the flank face
$\tilde{\sigma}_2$	normal stress at the cut-off point in Region II
τ_1	shear stress at the rake face
$\tau_{f_{1_{max}}}$	max. frictional shear stress along the tool rake face
$\tau_{f_{3_{max}}}$	max. frictional shear stress along the tool flank face
$\tilde{\tau}_2$	shear stress at the cut-off point in Region II

3. REVIEW OF FRICTION DETERMINATION METHODS

3.1 Pin-on-the-disc method

Rotating disc contacts a stationary pin tribometer. The ratio of the forces gives friction coefficient, which depends on temperature and pressure that cannot be achieved (Bonnet et al. 2008). Pin can follow cutting tool so that temperatures are maintained (Olsson et al. 1989, Hedenqvist&Olsson 1991), or the pin can be coated the same way as the cutting tool to maintain both temperature and pressure (Bonnet et al. 2008).

3.2 Gradient friction coefficient method

Graph of feed versus cutting force was found to have a linear trend at relatively higher feed rates, which shows that eq. (1) could be utilized to determine the friction coefficient (Arrazola&Meslin 2002, Arrazola et al. 2008).

$$\mu = tg\left(tg^{-1}\left(\frac{dF_f}{dF_c}\right) + \gamma_1\right) \qquad \text{Eq. (1)}$$

3. Mean friction coefficient method

Since the friction coefficient is quasi-steady along the friction surface, a mean value of the ratio of measured frictional force to cutting force could be used (Zorev 1963) (Eq. 2). This mean friction coefficient could be considered constant, or dependant on mean temperature (Moufki et al. 1998). Ploughing forces could be used to reformulate the mean friction coefficient (Eq. 3), or a similar method of reformulation could be done by subtracting the edge forces (Albrecht 1960, Sutter & Molinari 2005).

$$\mu = \frac{F_t}{F_c} \qquad \text{Eq. (2)}$$

$$\mu = \frac{F_t - F_{t_0}}{F_c - F_{c_0}} \qquad \text{Eq. (3)}$$

Another approach was to divide the friction coefficient into two components as apparent (μ_{ap}) and sliding (μ_{sl}) friction coefficients (Özlü et al. 2009, Molinari et al. 2011). Apparent friction coefficient is the ratio of total friction and normal forces on the entire rake face, where sliding friction coefficient is the ratio of the friction and normal forces acting on the sliding region along the rake face. Despite being more detailed than a single mean friction coefficient method, determination of the two friction coefficients is not applicable to the unstable nature of early stages of titanium and nickel based alloy machining.

4. DETERMINATION OF FRICTION FOR ROUND EDGE CUTTING TOOL

The tool-workpiece/chip interface during machining can be divided into three regions (Fig. 1), considering that the tool has a round edge, and is not worn. In Region 1, stick and slide conditions of friction are assumed where tool and workpiece have contact. In Region 2, only sliding friction occurs, and the forces change direction along the region. Flank wear is not considered to change the geometry of the tool, but when there is no flank wear (fresh tool), the contact of tool with the chip and workpiece ends after Region 2. When there is considerable flank wear, the contact between the tool and the workpiece will further go after Region 2, so a new contact of Region 3 is also introduced. In this region, only sliding friction is assumed.

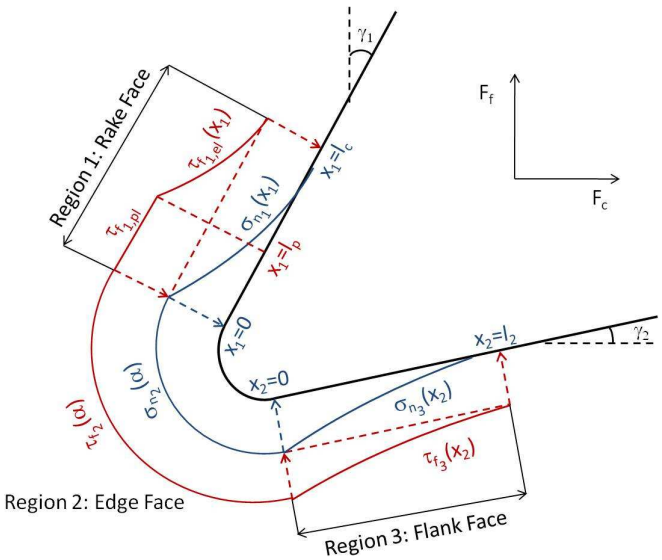

Figure 1: Illustration of stresses on the three regions of tool

To start the procedure, the unknown parameters (μ_1, μ_2, l_c, $\sigma_{n_{1_{max}}}$ & $\sigma_{n_{3_{max}}}$) are searched to calculate the tangential and normal force components. The forces that are found through this procedure are compared to the forces measured by the orthogonal cutting tests using same process parameters. The

searched parameters that make the difference between the calculated and measured forces the smallest are selected as the correct parameters.

In the first region, normal stress is assumed to start at a maximum level, and decay until it reaches zero at the end of tool-chip contact (Fig.2) (see Eq. 4). When this stress is integrated through the whole contact region along the rake face, the normal force in Region 1 can be found (Eq. 5). Since stick and slide conditions are assumed in this region, elastic and plastic shear stress values are calculated separately (Eq. 6), and the total tangential force in Region 1 can be found by integrating these frictional shear stresses along the contact (Fig.3).

$$\sigma_{n_1} = \sigma_{n_{1max}} \left(1 - \frac{x_1}{l_c}\right)^n \qquad \text{Eq. (4)}$$

$$F_{n_1} = \sigma_{n_{1max}} \frac{l_c}{n+1} \qquad \text{Eq. (5)}$$

$$\tau_{1(x)} = \begin{cases} \tau_{f_{1max}}, & 0 \le x \le l_p \\ \mu_1 \sigma_{1(x)}, & x > l_p \end{cases} \qquad \text{Eq. (6)}$$

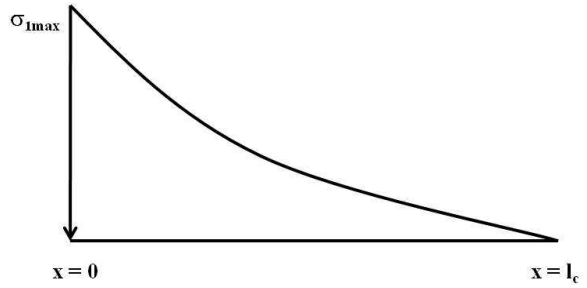

Figure 2: Normal stress along the rake face (Region 1)

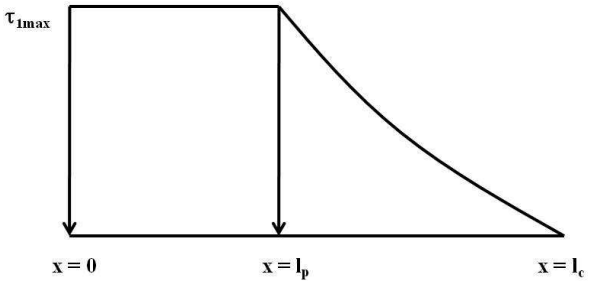

Figure 3: Shear stress along the rake face (Region 1)

In Region 2, normal and tangential stresses are assumed to change linearly throughout the angular profile (Fig. 4-6), and the normal and tangential forces are found by integrating the same way. The forces in Region 3 are calculated in a similar fashion to Region 1, except that there will be no sticking condition assumption here, and they will equal to zero when no contact is assumed (fresh tool).

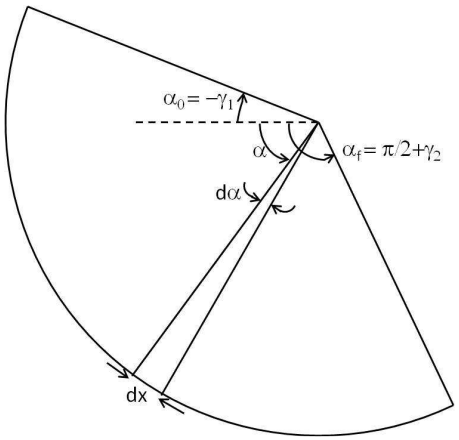

Figure 4: Edge face and angles (Region 2)

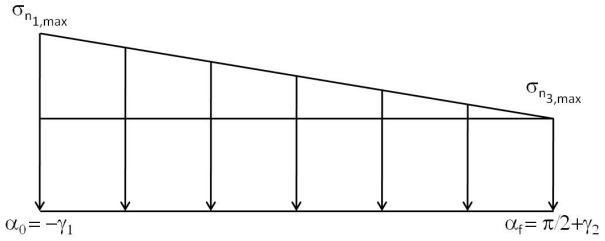

Figure 5: Normal stresses on the edge face (Region 2)

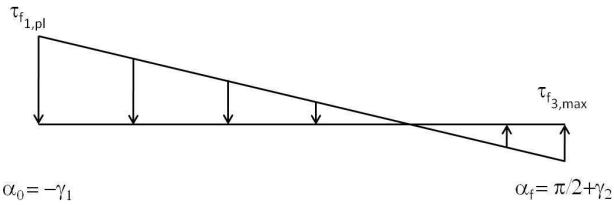

Figure 6: Shear stresses on the edge face (Region 2)

After all the forces are calculated, the cutting and friction forces are found by summing them up, and then experimental data is used to find the correct parameters. For Ti-64 alloy, test data of Wyen&Wegener (2010) is used, while for IN-100, test data of the authors is used. Non-linear relationships between the two friction coefficients (μ_1 & μ_2) and process parameters (V_c, t_u & r_β) are constructed (Eq. 7), and using the experimental data, the coefficients of these relationships are found (see Table 1 & 2).

$$\mu_i = a_i V_c + b_i t_u + c_i r_\beta + d_i V_c t_u + e_i V_c r_\beta + f_i t_u r_\beta + g_i V_c t_u r_\beta + h_i, \quad i = 1,2 \qquad \text{Eq. (7)}$$

It was found that for both materials, cutting edge radius was the parameter that affected the friction coefficients the most. The formula found using these coefficients could be utilized to predict friction coefficients during machining Ti-64 alloy in the ranges of V_c=10-110 m/min, t_u=0.06-0.2 mm, r_β=10-50 μm, and IN-100 alloy in the ranges of V_c=12-24 m/min, t_u=0.05-0.1 mm, r_β=10-25 μm.

Table 1: Coefficients of the non-linear relationships for rake and flank face friction coefficients for Ti-6Al-4V

	a	b	c	d	e	f	g	h
μ_1	-0.08	-0.12	0.5	0.01	0.02	-0.03	0.01	0.66
μ_2	0.04	0.12	-0.17	-0.03	-0.03	0.08	-0.02	1

Table 2: Coefficients of the non-linear relationships for rake and flank face friction coefficients for IN-100

	a	b	c	d	e	f	g	h
μ_1	-0.06	-0.13	0.58	-0.04	-0.01	-0.06	0.01	0.72
μ_2	0.05	0.15	-0.24	-0.13	0.05	0.04	0.06	0.98

5. DETERMINATION OF FRICTION FOR ROUND EDGE CUTTING TOOL IN PRESENCE OF TOOL FLANK WEAR

The machining process can also be modeled by considering a geometrical change in the tool due to tool wear. This is accurate for most machining processes, and especially for difficult-to-cut materials such as hardened steel, titanium and nickel alloys, because the tool wears very rapidly during machining. When the tool wears, it is believed that it is worn parallel to the cutting speed direction, and orthogonal to the feed direction. This creates another contact region at the flank face after the tool becomes worn, which divides the tool/workpiece contact into three basic regions as shown in Fig. 7.

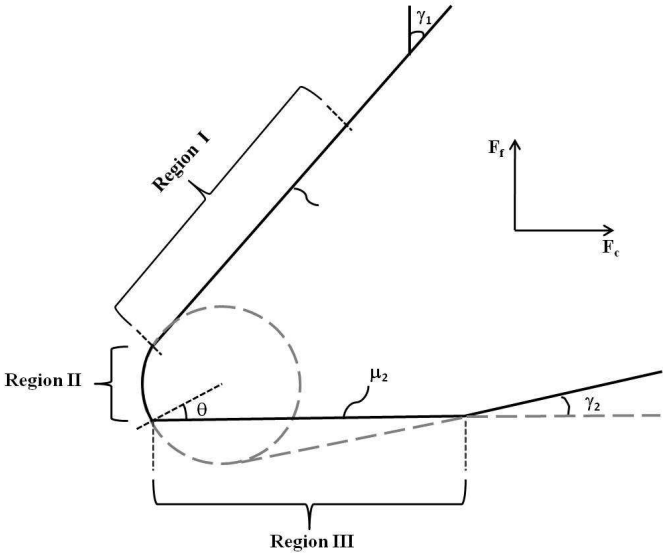

Figure 7: Illustration of the three regions of cutting edge of a tool in the presence of flank wear

The first contact region (Region I in Fig. 7) at the rake face of the cutting tool is modeled the same way as described in the previous section (see Fig. 2-3, Eq. 4-6). Since the change in the tool geometry after tool wear does not affect the rake face, there is no need to change the used model in this region. The forces in the normal and tangential directions are then found on the rake face by integrating the normal and tangential stresses along the region. When these forces are obtained, it is necessary to convert them into cutting speed and feed directions using cosine and sine of the rake angle. These converted values are compared to experimental measurements of machining forces. In order to do this conversion, it is necessary to use Eq. 8-11 to find the cutting and feed components of normal and tangential forces.

$$F_{n_{1_c}} = F_{n_1} \cos\gamma_1 \qquad \text{Eq. (8)}$$

$$F_{n_{1_f}} = -F_{n_1} \sin\gamma_1 \qquad \text{Eq. (9)}$$

$$F_{t_{1_c}} = F_{t_1} \sin\gamma_1 \qquad \text{Eq. (10)}$$

$$F_{t_{1_f}} = F_{t_1} \cos\gamma_1 \qquad \text{Eq. (11)}$$

The second contact region will be the edge face (Region II in Fig. 7). This is the curvilinear section that is located in between the linear rake region and the linear tool wear region (Fig. 8). The angle α in this region is the angle from the cutting speed (horizontal) direction. At the rake face end, the angle will be equal to the rake angle of the tool, but the direction will be negative. At the flank face end, the angle is calculated using to the clearance angle (γ_2), cutting edge radius (r_β), and the tool wear amount (*VB*) (Eq. 12). This angle can be called the cut-off angle for the edge face region. When the normal and shear stress equations are found, they will be integrated from α_0 to α_f to find the total forces on the edge face. However, in order to discuss stresses in this region, the stresses in the flank face should be investigated first, since the calculations for Region II depend on the results of flank face calculations.

$$\theta = \gamma_2 + \sin^{-1}\left(1 - \frac{VB\sin\gamma_2}{r_\beta}\right) \qquad \text{Eq. (12)}$$

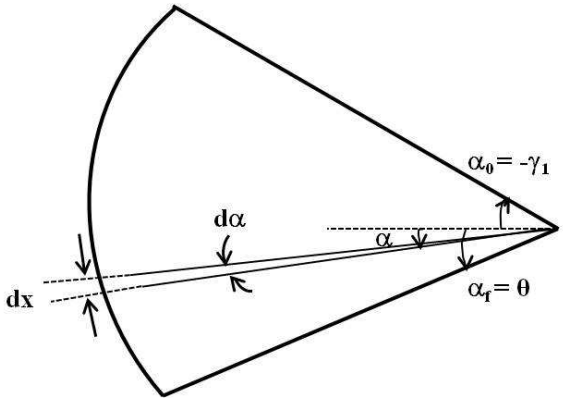

Figure 8: Tool edge face and angles (Region II)

The third contact region will be along the flank face (Region III in Fig. 7). This is the linear section that represents the tool flank wear. The tool is assumed to be worn, but for fresh tools, a very small tool wear length can be used to

represent freshness of the tool. The use of zero tool flank wear is not possible due to changes in calculation and also not advised because the tool wears very rapidly once the machining starts. At the beginning point of this region, the shear ($\tau_{f_{3max}}$) and normal ($\sigma_{n_{3max}}$) stresses will be at their maximum values, and they will decay as a power of the distance to become zero at x_3=VB (Fig. 9-10). The shear and normal stresses are related to each other with a friction coefficient different than the one between the tool and the chip at the rake face (μ_2), and this friction coefficient can be assumed constant along the flank face. After modeling the normal and shear stresses similar to those in the rake face region (Region I), a simple integration along the flank face contact length gives the corresponding forces (Eq. 13-14). This region is assumed to be parallel to the cutting speed direction, hence the normal stress can be used to find the feed force component in this region, and the shear stress can be used to find the cutting force component in this region, with no angular conversion needed.

$$F_{n_3} = \sigma_{n_{3max}} \left(\frac{VB}{m+1}\right) \quad \text{Eq. (13)}$$

$$F_{t_3} = \mu_2 \sigma_{n_{3max}} \left(\frac{VB}{m+1}\right) \quad \text{Eq. (14)}$$

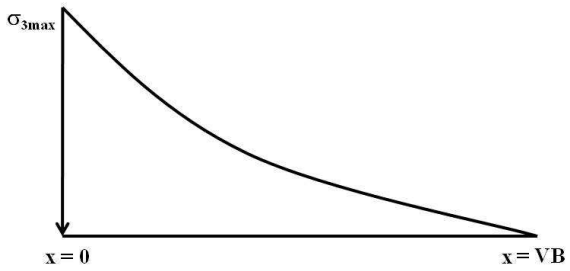

Figure 9: Normal stress along the flank face (Region III)

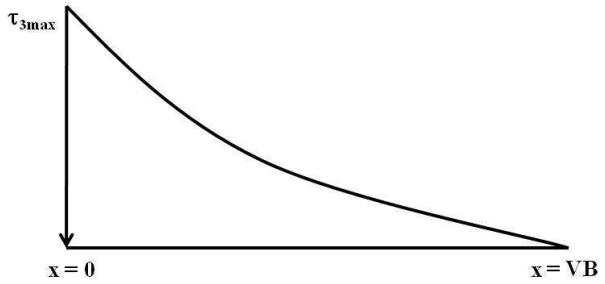

Figure 10: Shear stress along the flank face (Region III)

Now that the stresses in the third region are defined, one can go back to the discussion about the edge face stresses (Region II). In order to depict the stress distribution on the edge face, one needs to change from Cartesian to polar coordinates. Hence, the angle measured from the cutting velocity direction to the location on the edge face from the center of the edge radius is considered. Since the radius is constant in this region, the coordinate is converted into a linear picture (Figures 11-12). The normal stresses in the flank face region will be less than the normal stresses in the rake face due to the mechanics of cutting, so the maximum value of the normal stress at the flank face will be less than the maximum value at the rake face. This will mean that in the edge face, the normal stresses will decay from a higher value to a lower value, and this decay is assumed to be linear through the edge face (Fig. 11). The shear stresses, on the other hand, will be in the chip flow direction on the rake face, but will be in the negative cutting direction on the flank face (since the workpiece will be moving in that direction). This means that the frictional shear stress changes direction at the edge face (Fig. 12).

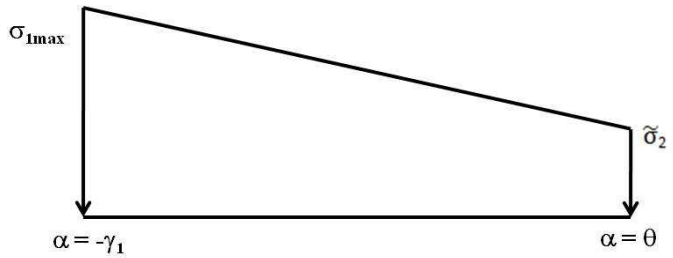

Figure 11: Normal stress along the edge face (Region II)

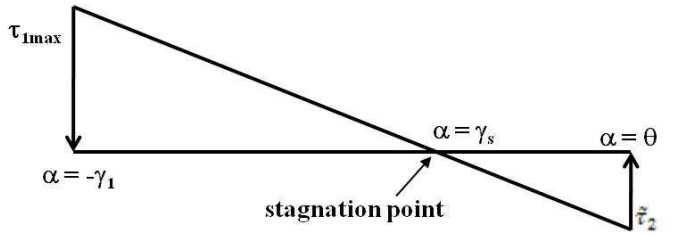

Figure 12: Shear stress along the edge face (Region II)

There have been many studies on determining the location of the stagnation point on the tool during machining, and the findings of these studies about stagnation angle show that this point falls on the edge face region depicted in Figures 7-8 (Fang 2003, Yen et al. 2004, Kishawy et al. 2006, Woon et al. 2008, Fang&Xiong 2008). Hence, at the location where the frictional shear stress changes direction, a stagnation point can be assumed and the stagnation angle (γ_s) can be calculated. The rake face maximum frictional shear stress will be assumed as the positive maximum value, and the flank face maximum frictional shear stress will be assumed as the negative maximum value of the frictional shear stress in the edge face region. The frictional shear stress in the edge face region will continuously decrease from a positive maximum value at the rake face end to a negative maximum value at the flank face end, and this decrease is assumed to be linear. Within this linearly decreasing region, the frictional shear stress value will be equal to zero at some point, which will be the stagnation point. Using the angle and frictional shear stress values, the angle of the stagnation point can be found as shown in Eq. (15). In this region, the normal and frictional shear stresses will be dependent on the angle α, so it is necessary to integrate these

forces with changing α angle along the edge face to find the normal and tangential forces.

$$\gamma_s = \frac{\theta\tau_{f1_{max}} - \gamma_1\tilde{\tau}_2}{\tau_{f1_{max}} + \tilde{\tau}_2} \quad \text{Eq. (15)}$$

There is continuity in geometry from the rake face (Region I) to the edge face (Region II), so the stresses should be continuous at that side as well. Hence, at the rake face end of the edge face region, the normal and shear stresses are equivalent to the stress values used for the rake face region, due to the continuity of the stresses. However, the geometry is not continuous at the beginning of the flank face, due to tool wear. At the end of the flank face, the vector sum of the shear and normal stresses at the flank face end should be equal to the vector sum of the shear and normal stresses at the beginning of the flank face, since they are essentially the same point (Eq. 16). From this, the components of the shear and normal stresses in the edge face region at the flank face border can be found using Eq. 17-18.

$$\overrightarrow{\tilde{\sigma}_2} + \overrightarrow{\tilde{\tau}_2} = \overrightarrow{\sigma_{n_{3_{max}}}} + \overrightarrow{\tau_{f_{3_{max}}}} \quad \text{Eq. (16)}$$

$$\tilde{\tau}_2 = \sigma_{n_{3_{max}}}(\mu_2 \cos\theta + \sin\theta) \quad \text{Eq. (17)}$$

$$\tilde{\sigma}_2 = \sigma_{n_{3_{max}}}(\mu_2 \sin\theta - \cos\theta) \quad \text{Eq. (18)}$$

Once all of the force components are calculated by integrating the normal and shear stresses and converting into the cutting and feed force components, they should be added up to find the resultant forces in the cutting and feed force directions (see Eq. 19-20). These correspond to the measurements from the orthogonal cutting tests, and they should be compared to find the right set of variables. The geometrical variables are the cutting edge radius (r_β), the rake angle (γ_1), the clearance angle (γ_2), and the tool flank wear angle (θ). The first three are geometrical constraints from the tool, and the last one will be calculated. The contact variables are the total tool-chip contact length (l_c), the plastic tool-chip contact length (l_p), and the tool flank wear length (*VB*). These are not known prior to the simulations, and should be searched at the initial iteration. The polynomial variables (*m, n*) are also not known and should be searched at the initial iteration (or they could be assumed a value for the first iteration). The stress variables (σ_{1max}, $\tilde{\sigma}_2$, σ_{3max}, τ_{1max}, $\tilde{\tau}_2$, τ_{3max}) are also not known prior to the first iteration, and they should be searched at the first iteration. However, the shear and normal stresses at the rake face and flank face regions are related to each other with the coefficients of friction, and the shear and normal stresses in the edge face region at the flank face end are calculated (Eq. 17-18). Hence, there are essentially only two stress variables (σ_{1max}, σ_{3max}) to search. Friction variables (μ_1, μ_2) are also not known and should be searched at every iteration (see Figure 13 for illustration of the algorithm).

$$F_c = F_{n_{1_c}} + F_{t_{1_c}} + F_{n_{2_c}} + F_{t_{2_c}} + F_{n_{3_c}} + F_{t_{3_c}} \quad \text{Eq. (19)}$$

$$F_f = F_{n_{1_f}} + F_{t_{1_f}} + F_{n_{2_f}} + F_{t_{2_f}} + F_{n_{3_f}} + F_{t_{3_f}} \quad \text{Eq. (20)}$$

At the initial iteration, all the unknown variables are searched within meaningful limits. For the friction coefficients, these limits were set initially as 0.1 and 0.95. For the stress variables, these limits were initially set as 100 and 10000 MPa. The contact lengths (l_c and l_p) were initially searched within the limits of [$1.0*t_u$, $4*t_u$] and [$0.5*t_u$, $3*t_u$], respectively. The initial limits were selected so that any physically possible condition is covered , and after focusing on approximate values, the limits of the search was changed to narrower values and reiterated for better accuracy. The polynomial variables are assumed to be 0.5, and they changed only slightly over the course of the next iterations. The values at each iteration are selected at random, and for each set of selection, forces in cutting and feed directions are found. These forces are compared to the measured forces from orthogonal cutting tests, and the error between the measured and calculated forces is used in the algorithm so that a total error is assigned to each set of variables (Figure 13). The selection of variables is done a satisfactory amount of times, and each random set of variables has an error assigned to it. The number of "satisfactory amount" is found through trial and error, and the optimum compromise between the computational time and result accuracy is determined. After enough number of sets are collected, the resultant variable set is found using Eq. (21), where x_R is the resultant variable, x_i is the i^{th} unknown (searched) variable, e_i is the error assigned to that variable, and *N* is the total number of variables.

$$x_R = \frac{\sum_{i=1}^{N} x_i/e_i}{\sum_{i=1}^{N} 1/e_i} \quad \text{Eq. (21)}$$

After the initial calculation of the unknown variables, the resultant variable set is passed to the Finite Element Modeling-based simulations. After a simulation is run until the forces are comparable to the measured forces, the stress fields at the rake and flank faces are extracted (Figure 13). When the stresses vs. the distances are fit to a power curve, the maximum normal ($\sigma_{n_{1_{max}}}$, $\sigma_{n_{3_{max}}}$) and frictional shear stresses ($\tau_{f_{1_{max}}}$, $\tau_{f_{3_{max}}}$) at the rake face and flank face regions as well as the polynomial coefficients (*m, n*) can be found. Also using the rake face stresses, one can find the total and plastic tool-chip contact lengths (l_c and l_p), and the stagnation point can be confirmed using the shear stress vector representation. At the next iteration of the friction determination method, these values will be used instead of searching for all of them. As a result, at each iteration after the initial iteration, the friction coefficients will be the only ones being searched (and then passed on to the FEM-based simulation model). When the friction coefficients are very close to each other within tolerable limits at two

consecutive iterations, the algorithm is stopped and the friction coefficients are determined (Figure 13).

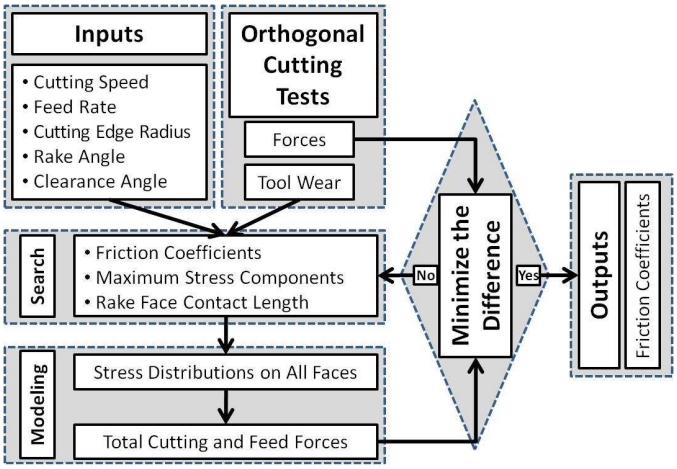

Figure 13: The search algorithm for the determination of friction coefficients

6. RESULTS AND VALIDATIONS

Simulation results for the nickel-based alloy IN-100 can be found in Table 3. The simulations were run for two different rake angles (0 and 3 degrees), two different edge radii (10 and 25 μm), two different cutting speed (12 and 24 m/min), and two different uncut chip thickness (0.05 and 0.1 mm), a total of 16 cutting conditions. Experimental results were gathered for all the conditions, as the cutting and tangential forces are used within the algorithm. The results presented in this table represents the last iteration, and the reason to stop the iterations was that in the previous iteration, the friction coefficients on the rake and flank faces (μ_1 and μ_2) were less than 0.01 different than the friction coefficients on the last iteration (shown in Table 4). As a result, it is safe to say that in all the cutting conditions, the friction coefficient on the rake face between the tool and the chip was 0.7, while the friction coefficient on the flank face between the tool and the worn workpiece was found to be around 0.62. Stagnation angle was found to be mostly dependant on the tool edge radius, and with increasing edge radius from 10 to 25 μm, the stagnation angle was found to increase from 10-15 degrees to 40-45 degrees. However, the tool wear was considered to be constant (60 μm) in all the conditions, which means that these simulations represent the values after a certain and similar tool wear amount, regardless of the cutting time or distance. Other process parameters did not affect the stagnation angle significantly.

Table 3: Search algorithm results compared to orthogonal cutting results for IN-100

						FDM Results		
	r_β	V_c	t_u	F_t	F_c	μ_1	μ_2	γ_s
γ_1=0	10	12	0.05	1185	1470	0.7	0.62	15.9
	10	12	0.1	1949	2166	0.7	0.62	14.2
	10	24	0.05	1090	1013	0.7	0.62	14.3
	10	24	0.1	1692	1602	0.7	0.62	12.2
	25	12	0.05	1074	967	0.7	0.62	45.6
	25	12	0.1	1756	1854	0.7	0.62	42.5
	25	24	0.05	882	707	0.7	0.62	43.6
	25	24	0.1	1415	1513	0.7	0.62	44.0
γ_1=3	10	12	0.05	768	885	0.7	0.62	13.7
	10	12	0.1	1292	1645	0.7	0.62	13.3
	10	24	0.05	810	932	0.7	0.62	13.6
	10	24	0.1	1298	1631	0.7	0.62	10.1
	25	12	0.05	941	1138	0.7	0.61	42.7
	25	12	0.1	1710	2217	0.7	0.62	45.2
	25	24	0.05	1094	1233	0.7	0.61	41.7
	25	24	0.1	1506	2255	0.7	0.62	40.1

Simulation results for the titanium-based alloy Ti-6Al-4V can be found in Table 4. The simulations were run for two different sets of experimentation. For higher cutting speed (V=120 m/min), the experimental results were received from the orthogonal cutting tests conducted at TechSolve Inc., and the depth of cut was b=5 mm. The experimental results for lower cutting speed (V=70 m/min) were extracted from the orthogonal cutting test results of Wyen&Wegener (2010), where the depth of cut was b=2 mm. Three different rake angles (0, 5, and 10 degrees), three different cutting edge radii (10, 20 and 30 μm), two different cutting speeds (70 and 120 m/min), and three different uncut chip thickness (0.05, 0.06 and 0.1 mm) were used. However, the intention was to make the low feed values as close to each other as possible, as the two different measurement sets did not have two lower values of uncut chip thickness. The two low values are very close to each other, and the difference in the effect can be assumed statistically non-significant. In total, it is possible to see the effect of all four cutting parameters in 8 experiments/simulations.

It can be observed from Table 4 that none of the parameters had any significant effect on the friction coefficients, and the rake face friction coefficients were found to be around 0.6 for all the parameters used. The flank face friction coefficient was also constant around 0.51, except for the highest cutting edge radius (30 μm), where it dropped slightly to 0.45-0.49. The stagnation angle was found to decrease slightly with increasing feed, and not change significantly with cutting speed or the rake angle. As with the nickel-based alloy IN-100, the stagnation angle during machining the titanium-based alloy Ti-64 also depended heavily on the edge radius, and with edge radius increasing from 10 to 20 and 30 μm, the stagnation angle increased from around 10 degrees to 27 and 45 degrees respectively.

Table 4: Search algorithm results compared to orthogonal cutting results for Ti-64

						FDM Results		
	r_β	V_c	t_u	F_t/b	F_c/b	μ_1	μ_2	γ_s
[illegible]	10	120	0.05	51	104	0.60	0.51	11.3

	10	120	0.1	80	189	0.59	0.51	8.8
γ_1=5	10	120	0.05	48	99	0.60	0.52	12.0
	10	120	0.1	67	180	0.60	0.52	8.6
γ_1=10	20	70	0.06	75	128	0.59	0.51	28.1
	20	70	0.1	83	188	0.58	0.51	25.8
	30	70	0.06	110	139	0.59	0.45	45.3
	30	70	0.1	113	191	0.59	0.49	45.0

7. CONCLUSIONS

Since friction plays an important role in machining processes, this work introduced a new iterative technique to determine the friction coefficients and related parameters during machining titanium- and nickel-based alloys. Experimental results from various sources were used as guidance, since the experimental cutting forces are needed to initiate the iterative algorithm. Two different techniques were introduced, one with constant tool geometry, and the other one with worn tool geometry, and the results were reflected to show the friction coefficients and related parameters under different cutting parameters. It was found that while the friction coefficients did not depend on most of the cutting parameters, they changed with changing workpiece material, and slightly with cutting edge geometry. With both methods introduced, rake and flank face friction coefficients were found to be similar for Ti-6Al-4V. This methodology can be used to determine the friction coefficient for simulations in DEFORM or any other FEM software, and the methodology also offers to be expanded to other materials and cutting parameters via gathering of more orthogonal cutting tests.

8. ACKNOWLEDGMENTS

This project was supported by the NSF grant CMMI- 1130780.

9. REFERENCES

Albrecht P. “New Developments in the Theory of the Metal-Cutting Process.” *Transactions of the ASME – Journal of Engineering for Industry* (1960): 348-358.

Arrazola P. & Meslin F. “A Technique for the Identification of Friction at Tool/Chip Interface during Machining.” *Proceedings of the Second Asia International Conference on Tribology* (2002).

Arrazola P., Ugarte D. & Domínguez X. “A New Approach for the Friction Identification during Machining Through the Use of Finite Element Modeling.” *International Journal of Machine Tools & Manufacture* 48 (2008): 173-183.

Bonnet C., Valiorgue F., Rech J., Claudin C., Hamdi H., Bergheau J.M. & Gilles P. “Identification of a Friction Model – Application to the Context of Dry Cutting of an AISI 316L Austenitic Stainless Steel with a TiN Coated Carbide Tool.” *International Journal of Machine Tools & Manufacture* 48 (2008): 1211-1223.

Fang N. “Slip-Line Modeling of Machining with a Rounded-Edge Tool – Part II: Analysis of the Size Effect and the Shear Strain-Rate.” *Journal of the Mechanics and Physics of Solids* 51 (2003): 743-762.

Fang N. & Xiong L.S. “Determination of Friction and Material-Flow Boundary Conditions on the Tool Round Cutting Edge.” *Transactions of NAMRI/SME* 36 (2008): 413-420.

Hedenqvist P. & Olsson M. “Sliding Wear Testing of Coated Cutting Tool Materials.” *Tribology International* 23.3 (1991): 143-150.

Kishawy H.A., Haglund A.J. & Deiab I.M. “An Analysis of Machining with Honed Tools Using ALE Finite Element Model: Ploughing Force and Minimum Chip Thickness.” *Transactions of NAMRI/SME* 34 (2006): 277-284.

Molinari A., Cheriguene R. & Miguelez H. “Numerical and Analytical Modeling of Orthogonal Cutting: The Link between Local Variables and Global Contact Characteristics.” *International Journal of Mechanical Sciences* 53 (2011): 183-206.

Moufki A., Molinari A. & Dudzinski D. “Modelling of Orthogonal Cutting with a Temperature Dependent Friction Law.” *Journal of the Mechanics and Physics of Solids* 46.10 (1998): 2103-2138.

Olsson M, Soderberg S., Jacobson S. & Hogmark S. “Simulation of Cutting Tool Wear by a Modified Pin-on-Disc Test.” *International Journal of Machine Tools & Manufacture* 29.3 (1989): 377-390.

Özlü E., Budak E. & Molinari A. “Analytical and Experimental Investigation of Rake Contact and Friction Behavior in Metal Cutting.” *International Journal of Machine Tools & Manufacture* 49 (2009): 865-875.

Sutter G. & Molinari A. “Analysis of the Cutting Force Components and Friction in High Speed Machining.” *Journal of Manufacturing Science and Engineering* 127 (2005): 245-250.

Woon K.S., Rahman M., Neo K.S. & Liu K. “The Effect of Tool Edge Radius on the Contact Phenomenon of Tool-Based Micromachining.” *International Journal of Machine Tools & Manufacture* 48 (2008): 1395-1407.

Wyen C.-F., Wegener K. “Influence of Cutting Edge Radius on Cutting Forces in Machining Titanium.” *CIRP Annals – Manufacturing Technology* 59 (2010): 93-96.

Yen Y.C., Jain A. & Altan T. “A Finite Element Analysis of Orthogonal Machining Using Different Tool Edge Geometries.” *Journal of Materials Processing Technology* 146 (2004): 72-81.

Zorev N.N. “Interrelationship between Shear Processes Occurring Along Tool Faces and on Shear Plane in Metal Cutting.” *International Research in Production Engineering, Proceedings of the International Production Engineering Research Conference* (1963): 42-49.

